Research Article
Hittite Journal of Science and Engineering, 2023, 10 (3) 229–235
ISSN NUMBER: 2149–2123
DOI: 10.17350/HJSE19030000311

Cobalt Boride (Co_2B) Particle Synthesis by One-step Carbothermic Reduction

Levent Kartal
Hitit University, Department of Metallurgical and Materials Engineering, Corum, Türkiye

ABSTRACT

In this study, crystalline Co_2B powder production was carried out by a one-step carbothermal reduction method starting from cheap, easily accessible oxide-based materials. Firstly, to determine the carbothermic Co_xB formation conditions, the decomposition temperatures of the raw materials were analysed by TG/DTA, and the temperature-varying Gibbs free energies of the expected reactions were calculated. Then, Co_2B production was carried out at constant $CoO/B_2O_3/C$ (3.22/1.5/1.3) weight ratios at temperature (1273-1473 K) and time (30-270 min). Scanning electron microscopy (SEM), X-ray diffraction (XRD), and vibrating sample magnetometer (VSM) were used to characterize the particles. XRD results showed that reaction temperature and time are the primary control on Co_xB formation and single-phase crystalline Co_2B particles with crystallite sizes of 88 nm were successfully produced at 1473 K and 150 min. The permanent magnetization, saturation magnetization, and coercivity values of Co_2B particles were defined as 16.58 Oe, 35.361 emu/g, 0.501 emu/g, respectively.

Keywords:
Cobalt boride, cobalt, carbothermic reduction, cobalt alloy

Article History:
Received: 2023/03/31
Accepted: 2023/07/04
Online: 2023/09/30

***Correspondence to**: Levent Kartal,*
E-Mail: leventkartal@hitit.edu.tr
Phone: +9 0 364 2191200
Fax: +90 364 2191310

This article has been checked for similarity.

INTRODUCTION

Cobalt is a crucial component used in industrial, military, and medical uses [1-3]. The most crucial utilization parts of cobalt and its alloys are super alloys, batteries, catalysts, magnetic alloys, high-speed steels, and cemented carbides [4]. In recent years, among Co alloys, cobalt borides (Co_xB) stand out with their high hardness, excellent wear resistance and superior magnetic and catalytic properties. Due to these superior properties, studies have been carried out on using cobalt borides in many areas, such as improving prosthetic alloys' corrosion and wear properties, and catalyst material for hydrogen production systems and fuel cells [5-9].

The production of Me_xB can be accomplished using a variety of processes, such as the direct solid-state reaction of elements [10-12], chemical reduction [13-15], molten salt electrolysis [16-18], mechanochemical [19], and electric arc technique [20]. The corrosion and wear resistance of cobalt-based alloys (CoCrMo) used in producing orthopaedic prostheses is provided by thin boride films formed on the surface. The boride film on the surface of these alloys is formed by a molten salt electrolysis and thermochemical processes [5-7]. Ruiz et al. [21] formed a boride film on the surface of CoCrMo alloys by thermochemical processes and observed that hardness and tribo-corrosion properties increased. Co_xB compounds are also used to enhance the surface properties of mild steels owing to their high hardness and wear resistance. Baris et al. [22] coated the surface of S235JRC carbon steel with mechanochemically produced Co_2B particles using a laser and investigated its machinability properties. In addition to improving surface properties, it is also used as reinforcing particles in metal matrix composites. Khoshsima et al. [23] used CoB-TiB_2 particles produced by chemical reduction to improve the properties of parts produced from Ti6Al4V particles by additive manufacturing. Co_xB particles have drawn attention in recent years, particularly with their catalytic properties in hydrogen production and storage, and studies in this field have intensified. The production of particles for catalyst applications of hydrogen storage and production systems is carried out using high-temperature solid-state synthesis, chemical reduction and mechanochemical methods starting from elemental Co and B [8-15,19,20, 24, 25].

Most methods used in producing cobalt boride (Co_2B) particles are unsuitable for industrial production due to limitations such as high raw material cost, multi-step and long experimental procedures, and high-cost specialized equipment requirements. Industrial ma-

Cite as:
Kartal L, "Cobalt boride (Co2B) particle synthesis by one-step carbothermic reduction". Hittite J Sci Eng. 2023;10 (3): 229-235. doi:10.17350/hjse19030000311

nufacturing prefers simple, quick synthesis processes with minimal production costs. In producing metal borides, carbothermic reduction stands out with its low cost, one-step, simple and fast production possibilities [26, 27]. The most well-known example of the carbothermic reduction in metal boride production is ferrobor (FeB) production. Ferrobor, used as an additive in the iron and steel industry, has been produced by the carbothermic reduction method for a long time [28, 29]. In this method, metal oxide and a B_2O_3/H_3BO_3 combination are heated with carbon to produce carbothermic metal borides. The most significant parameters in carbothermic metal boride production are the Me:B ratio of the oxide mixture, temperature, and reaction time.

In this study, the synthesis of crystalline single Co_2B phase particles by a simple, fast and one-step carbothermic reduction process was carried out using CoO, B_2O_3 and C. Thermo-gravimetric/differential thermal analysis (TG/DTA) analysis of the raw material and the Gibbs free energy change graphs of the reactions with temperature were used to determine the mechanism of Co_xB formation. The phase structure of Co_2B particles was studied in detail by XRD, morphology by SEM and magnetic properties by VSM.

MATERIAL AND METHODS

In the synthesis of Co_xB powder, cobalt oxide (CoO) was used as Co resource, diboron trioxide (B_2O_3) (>97%) as B resource and carbon (>99%) as a reductant. Stoichiometric weight ratios of constant $CoO/B_2O_3/C$ were used as 3.22/1.5/1.3 in the experiments. The investigated process parameters are summarized in Table I.

Table 1. Experimental parameters of carbothermic Co_xB synthesis.

Group	*Weight ratio (CoO/B2O3/C)*	*Parameter*	*Experiment conditions*	*Variables*
I	*3.22/1.5/1.3*	*Temperature*	*150 min*	*1273 K, 1373 K, 1473 K*
II		*Time*	*1473 K*	*30 min, 150 min, 270 min*

Before the synthesis, the powders constituting the raw material were mixed using agate mortar. Then powder mixture was fed into the furnace in alumina boats. The experiments were conducted under an argon atmosphere, and the argon flow was constant at 0.5 L/min during heating, reaction, and cooling. Each experiment's heating rate was 283 K / minute. The synthesis steps and schematic depiction of the experimental setup are shown in Fig. 1.

After synthesis, the products were leached with hot water to remove unreacted compounds and dried at 353 K for 2 hours.

The analyses of the raw materials and obtained products was carried out using thermo-gravimetric/differential

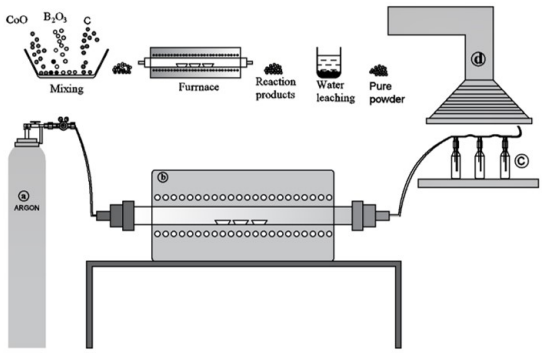

Figure 1. Schematic depiction of the experimental setup (a) argon cylinder (b) furnace (c) gas washing bottle (d) fume hood.

thermal analysis (TGA/DTA-HITACHI-STA7300), X-Ray diffractometer (XRD-(PANalytical X-Pert3 Powder)), scanning electron microscopy (SEM- ZEISS EVO LS 10) and vibrating sample magnetometer (VSM-Lake Shore 7407). Gibbs free energy (ΔG) values of the predicted reactions obtained with the help of HSC 5.1 software.

To calculate the crystal size of single-phase particles, the Scherrer equation was utilized. Scherrer equation for the calculation of particle crystal size is;

$$\boldsymbol{D = k\lambda / \beta \cos\theta} \quad (1)$$

where β is the Full width at half maximum (FWHM) of the peak, θ is the Bragg angle, λ is the wavelength of the used X-ray beam (1.54), and K is the Scherrer constant [30].

RESULTS AND DISCUSSION

Carbothermic synthesis mechanism of Co_xB

TG/DTA results and Gibbs free energy (ΔG) values of the predicted reactions were used to determine the carbothermic Co_xB synthesis mechanism. Firstly, the thermal behaviour of the mixed powders was investigated at a warming rate of 283 K/min to determine the thermal decomposition temperatures. The obtained TG/DTA curve is given in Fig. 2. In the TG graph, a low weight decrease occurred initially due to moisture loss of the powder mixture and then little weight change was observed up to 900 K. Between 900-1173 K the weight change increased compared to the weight change between 473-900 K. Above 1173 K, a sharp weight loss was observed, which may be due to the formation of CO gas. Four typical endothermic peaks were identified in the DTA curve given in Fig. 2. The first endothermic peak occurred at 404 K because of the removal of the water contained in the mixture. Second, endothermic peaks at 1109 K are believed to be caused by the reduction of the powder mixture, such as Co and B from CoO and B_2O_3, while the third endothermic peaks at 1172 K are thought to be due to the formation of the Co_2B phase and fourth peak at 1226 is thought to be due to the formation of the CoB. TG/DTA analysis reve-

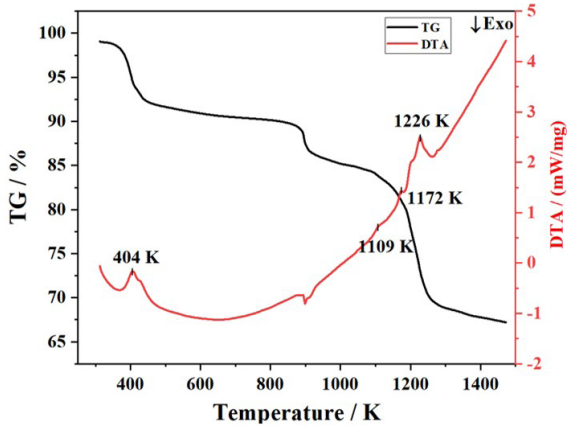

Figure 2. TG/DTA curves of $CoO/B_2O_3/C$ at warming rate of 20 °C min^{-1}.

als that the appropriate carbothermic synthesis temperature for producing Co_xB using the $CoO/B_2O_3/C$ powder mixture is above 1226 K.

In addition to the TG/DTA analysis, the Gibbs free energies of the predicted reactions were calculated to determine the mechanism of Co_xB formation. The temperature-dependent Gibbs free energy changes of the reactions are given in Fig. 3. Carbothermic CoB production proceeds in the following steps:

$$CoO + C = Co + CO_{(g)} \quad (2)$$

$$B_2O_3 + 3C = 2B + 3CO_{(g)} \quad (3)$$

$$4CoO + B_2O_3 + 7C = 2Co_2B + 7CO_{(g)} \quad (4)$$

$$2CoO + B_2O_3 + 5C = 2CoB + 5CO_{(g)} \quad (5)$$

When the graph in Fig. 3 is examined, it is seen that CoO can be reduced via C thermodynamically at 773 K, Co_2B can be produced at 1033 K, and CoB can be synthesized at 1218 K and higher temperatures.

Fig. 3 reveals that CoO will undergo reduction first in accordance with reaction (2). The carbothermic reduction of B_2O_3 alone (3) is not thermodynamically possible at the

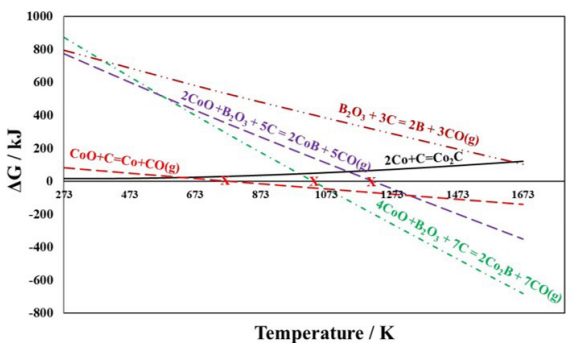

Figure 3. Gibbs free energies of reactions (2)–(5) change with temperature.

proposed reaction temperatures. The carbothermic reduction of B_2O_3 in the presence of CoO to form Co_2B and CoB according to reactions (4) and (5) appears to occur. Considering the Co-B diagram and the literature, stable Co_xB compounds were identified, and according to these compounds' formation reactions were deduced [31]. Co_xB production proceeds in the following steps:

$$2Co + B = Co\ B \quad (6)$$

$$Co + B = CoB \quad (7)$$

$$Co_2B + B = 2CoB \quad (8)$$

$$CoB + Co = Co_2B \quad (9)$$

The temperature-varying Gibbs free energy of the formation graph of the proposed reactions is given in Fig. 4. Diffusion-based thermochemical synthesis of Co_xB occurs by diffusion of B into Co particles with the driving force of B concentration gradient and temperature (equations 6-9). The first product formed on the surface of Co particles by B diffusion is thermodynamically always the boride compound (Co_2B) with the lowest mole fraction of boron (equation 6). With increased B diffusion on the Co_2B surface, Co_2B is converted into CoB (equation 8). With sufficient time allowed for B diffusion, Co_2B transforms into CoB, while CoB reacting with Co in the particle centre forms Co_2B again (equation 9).

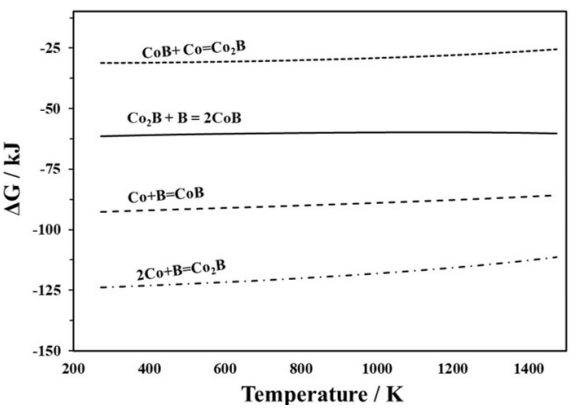

Figure 4. Gibbs free energies of reactions (6)–(9) change with temperature.

Carbothermic synthesis mechanism of Co_xB

From the TG/DTA analyses given in Fig. 2 and the Gibbs free energy of formation graphs of the reactions given in Fig. 3, it is seen that CoB conversion occurs at 1218 K and above. Therefore, the influence of temperature on Co_xB synthesis was thermodynamically investigated at temperatures of 1273, 1373 and 1473 K above the CoB formation temperature of 1218 K.

The phase structures of the particles were synthesized at different temperatures for 150 minutes were investigated

by XRD and given in Fig. 5. According to the XRD patterns in Fig. 5, unreacted oxidized phases were found besides Co at 1273 K, while the particles synthesized at 1373 K were found to consist only of the Co phase. When the temperature was boosted to 1473 K, the conversion to Co_xB increased, and Co_2B formed the main phase structure in the particles. Temperature increase improves B diffusion. The Co and Co_2B phases produced at 1173 K on the surface were changed into CoB by raising the temperature to 1273 K, according to Calik et al. [2]. At 1473 K, almost all Co phases obtained at 1273 and 1373 K transformed into Co_2B.

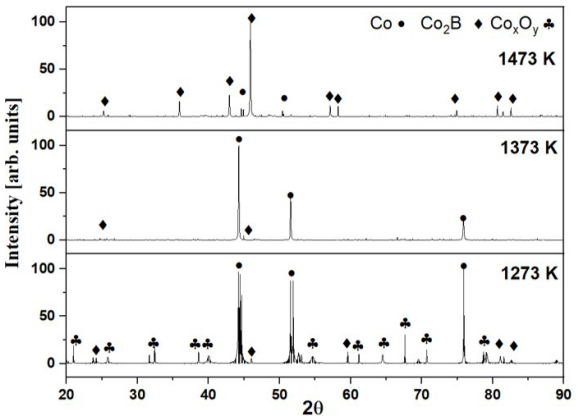

Figure 5. XRD patterns of Co-CoxB particles synthesized at different temperatures for 150 min.

SEM was used to investigate effects of temperature on particle morphology. Fig. 6 shows the detailed morphology of Co-Co_xB powders obtained at different temperatures. From the images in Fig. 6, it is understood that the particles were formed in a vast size range, spherical morphology and due to agglomeration of fine-grained particles.

Under 1473 K, no significant Co_xB synthesis occurred, and only CoO was reduced. Therefore, the images given in Figs. 6a and 6b represent mainly Co particles. By increasing the temperature to 1473 K, 88 nm crystal size single phase Co_2B particles were synthesized. No significant change in particle morphology was observed with increasing the temperature to 1473 K.

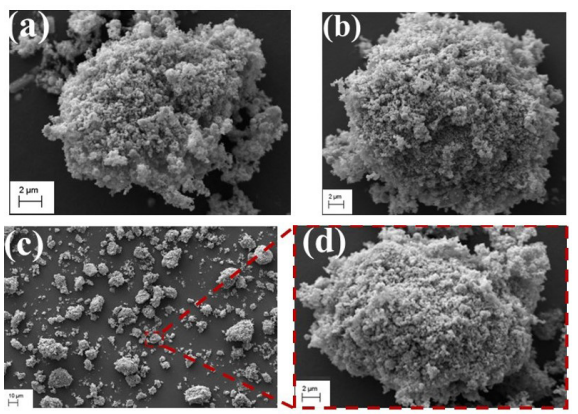

Figure 6. SEM images of Co-CoxB particles produced for 150 min at different temperatures: (a) 1273 K, (b) 1373 K, (c) 1473 K.

Effect of process duration on Co_xB particles

In diffusion-based thermochemical synthesis processes, reaction time and temperature are the most critical parameters. Diffusion of B increases with duration [5]. The effect of reaction time on particle structure and morphology was investigated at 30, 150 and 270 min. To ascertain the phase transition, the investigates were conducted at a constant temperature of 1473 K, where considerable CoxB phase synthesis took place. XRD patterns of particles synthesised at three different times are given in Fig. 7. The results of the XRD analysis confirmed that the particles only contained Co because B diffusion did not take place in adequate amounts in them over a short period of time (30 min). When the time was extended to 150 min to obtain single phase Co_xB, it was determined that the Co_2B phase replaced the main Co phase seen at the end of the 30 min, and the particles contained only the Co2B phase. Then, to obtain the CoB phase by increasing B diffusion, the time was extended to 270 min. At the end of 270 min reaction time, it was observed that the particles obtained consisted of Co_2B and CoB as expected. At the end of 270 minute, the coexistence of Co, Co_2B and CoB phases in the powder supports the predicted diffusion-based synthesis and indicates that the diffusion-based synthesis takes place in the form of Co-Co_2B and CoB [5, 6]. It is estimated that the possible reason for the presence of metallic cobalt, which does not form boride in the structure despite the long test times, is the removal of boron oxide compounds with low evaporation temperature from the system by evaporation.

Fig. 8 shows the morphology of the particles obtained at different times. It was shown that the particles obtained at all times directed similar formation mechanisms, and the accumulation of nanoparticles produced the secon-

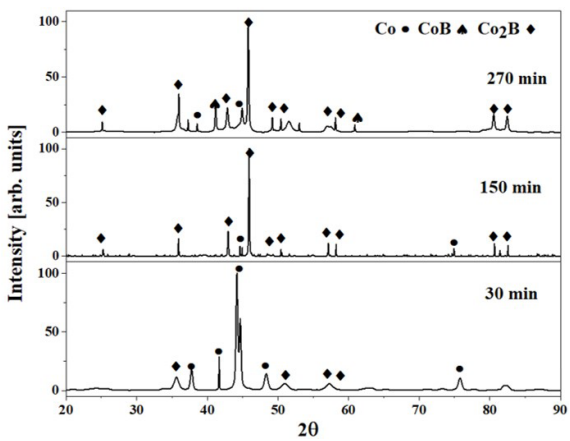

Figure 7. XRD patterns of Co-Co_xB powders produced at constant 1473 K for different durations.

dary large-sized particles. It has been seen that single-phase nanocrystalline Co_2B particles with a crystal size below 100 nm can be produced carbothermically in a single step from inexpensive starting materials. It is understood that carbothermic synthesis produces lower sized particles than calciothermic produced Co_2B particles, while chemical reduction processes produce larger sized particles. Simsek et al. [15] reported that Co_2B particles with particle sizes ranging between 30-100 nm were produced by chemical reduction. Baris et al. [33] succeeded in producing nanocrystalline Co_2B particles with a crystal size of approximately 10 nm by mechanochemical method using Co, B_2O_3 and Mg. Kartal [16] produced Co_2B particles calciothermically in molten salt medium starting from CoO and B_2O_3 and stated that the particle sizes are very variable but above 10 microns.

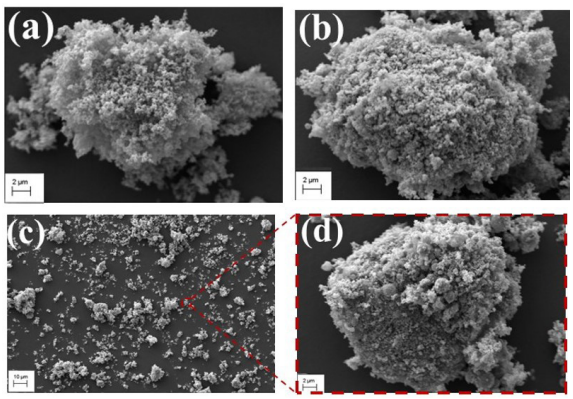

Figure 8. SEM images of Co-Co_xB powder synthesized at 1473 K for different durations: (a) 30 min, (b) 150 min, (c) 270 min.

The magnetic behaviour of Co_2B powders were investigated at ambient temperature in the range of ±20 kOe using VSM. The magnetization curve given in Figure 9 shows that Co_2B powders show soft magnetic behaviour under a magnetic field and draw ferrimagnetism-like hysteresis. It was defined that the saturation magnetization value of the powder was Ms=35.361 emu/g, the coercive magnetization value was Hc=16.58 Oe, and the permanent magnetization value was Mr=0.501 emu/g. It was observed that Co_2B particles produced by different methods showed similar magnetic properties. Kartal [16] reported the saturation magnetisation, coercivity and permanence values of the particles produced calciothermically starting from B_2O_3 and CoO as 30.107 emu/g, 40.210 Oe, 0.764 emu/g, respectively. Baris et al. [33] found that the saturation magnetisation values of the particles produced magnesiothermically using Co and B_2O_3 varied between 35 and 50 emu/g. Şimşek et al. [15] observed that the saturation magnetisation values of the particles produced by chemical reduction with the use of high purity starting materials varied between 19 and 68.5 emu/g depending on the calcination medium. Besides the production method, particle size is also effective on magnetic properties. Petit et al. [32] investigated the size-dependent magnetic properties of nanoscale Co_xB particles. The study reported that the magnetic behaviour could shift from ferromagnetic to superparamagnetic depending on the particle size, and Ms values increase with decreasing particle size. While the Ms value of particles with a 2.5 nm size was 70 emu/g, the Ms value of particles above 10 nm was 35 emu/g, like this study.

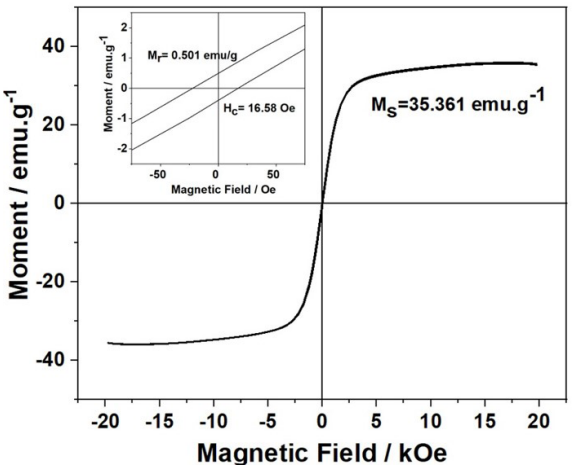

Figure 9. Magnetization curves of Co2B powders produced at constant1473 K temperature for 150 min.

CONCLUSION

This study investigated single-phase, nanocrystalline Co_2B particles production by carbothermic reduction using low-cost, oxide-based starting materials. The effect of temperature (1273-1473 K) and time (30-270 min) on Co_2B production was investigated at constant weight ratios of $CoO/B_2O_3/C$ (3.22/1.5/1.3). The experimental results obtained are summarised as follows;

a) XRD analyses showed that the synthesis of CoxB occurred in the form of Co-Co_2B-CoB as predicted by thermodynamic calculations.
b) As a result of XRD results, it was determined that B diffusion increased with the rise in temperature and time, and the production of single Co_2B phase particles occurred at 1473 K temperature and 150 min time.
c) SEM images showed that micron-sized secondary particles with irregular morphology were formed due to the agglomeration of nano-sized primary particles.
d) Single-phase nanocrystalline Co_2B particles with a crystal size of 88 nm showed high agglomeration tendencies.
e) Saturation magnetisation, permanent magnetisation and coercivity values of Co_2B particles were determined as 35.361 emu/g, 16.58 Oe, 0.501 emu/g, respectively.

CONFLICT OF INTEREST

The author deny any conflict of interest.

REFERENCES

1. Fisher KG. Cobalt Processing Developments, in: The Southern African Institute of Mining and Metallurgy. Paper presented at 6th South African Base Metals Conference, Marshalltown, 21-22 July, SAIMM, Rosebank, pp. 237–258, 2011.
2. Crundwell FK, Moats MS, Ramachandran V, Robinson TG, Davenport WG. Cobalt – Occurrence, Production, Use and Price, in: Crundwell FK, Moats MS, Ramachandran V, Robinson TG, Davenport WG (Eds.) Extractive Metallurgy of Nickel, Cobalt and Platinum Group Metals, Elsevier, Amsterdam, pp. 357–63, 2011
3. Mégret A, Vitry V, Delaunois F. Study of the processing of a recycled WC–Co powder: can it compete with conventional WC–Co powders Journal of Sustainable Metallurgy 7 (2021) 448–458.
4. Roberts S, Gunn G. Cobalt, in: Gunn G. (Eds). Critical metals handbook, Wiley, New York, pp. 122–49, 2013.
5. Campos-Silva I, Franco-Raudales O, Meda-Campaña JA, Espino-Cortés FP, Acosta-Pavón JC. Growth kinetics of CoB-Co2B layers using the powder-pack boriding process assisted by a direct current field. High Temperature Materials and Processes 38 (2019) 158–67.
6. Çalik A, Karakas MS, Ucar N, Ünüvar F. Boriding kinetics of pure cobalt. Kovove Materialy 52 (2014) 107–12.
7. Rodríguez-Castro GA, Reséndiz-Calderon CD, Jiménez-Tinoco LF, Meneses-Amador A, Gallardo-Hernández EA, Campos-Silva IE. Micro-abrasive wear resistance of CoB/Co2B coatings formed in CoCrMo alloy. Surface and Coatings Technology 284 (2015) 258–63.
8. Lv J, Wang Q, Zhao J, Liu W, Chen P, Liu H. The difference in the improvement of electrochemical hydrogen storage performance between two methods of coating copper on the surface of Co2B alloy. Chemical Physics Letters 754 (2020) 137697.
9. Altıntaş Z, Khoshsima S, Schmidt M, Bobnar M, Burkhardt U, Somer M, et al. Evolution of magnetic properties of crystalline cobalt-iron boride nanoparticles via optimization of synthesis conditions using hydrous metal chlorides. Journal of Magnetism and Magnetic Materials 523 (2021) 1–8.
10. Oh JH, Kim M, Lee YH, Hong SH, Park SS, Kim TH, et al. Synthesis of cobalt boride nanoparticles and h-BN nanocage encapsulation by thermal plasma. Ceramics International 46 (2020) 28792–9.
11. Lv J, Wang Q, Chen P, Liu H, Su Z, Zhao J, et al. Effect of ball-milling time and Pd addition on electrochemical hydrogen storage performance of Co2B alloy. Solid State Sciences 103 (2020) 106184.
12. Niu X, Wang X, Guan K, Wei Q, Liu H. Preparation, and electrochemical hydrogen storage application of mesoporous carbon CMK-3 coated Co2B alloy composite. Chemical Physics Letters 778 (2021) 138762.
13. Ghafar FA, Etherton D, Liu S, Buckley CE, English NJ, Silvester DS, et al. Tuning the catalytic activity of bifunctional cobalt boride nanoflakes for overall water splitting over a wide pH range. Journal of The Electrochemical Society 169 (2022) 096507.
14. Masa J, Weide P, Peeters D, Sinev I, Xia W, Sun Z, et al. Amorphous cobalt boride (Co2B) as a highly efficient nonprecious catalyst for electrochemical water splitting: oxygen and hydrogen evolution. Advanced Energy Materials 6 (2016) 1502313.
15. Simsek T, Barış M. Synthesis of Co2B nanostructures and their catalytic properties for hydrogen generation. Journal of Boron 2(1) (2017) 28–36.
16. Kartal L. Synthesis of cobalt boride particles by molten salt assisted calciothermic reduction. Transactions of the Indian Institute of Metals 76(3) (2022) 757–764.
17. Kartal L. Single Fe2B Phase Particle Production by Calciothermic Reduction in Molten Salt. Hittite Journal of Science and Engineering 9(2)(2022) 145–50.
18. Kartal L. Single step calciothermic synthesis of nickel boride particles in molten salt. Journal of the Australian Ceramic Society (2023) https://doi.org/10.1007/s41779-023-00893-9.
19. Sharifi H, Rabiei Faradonbeh S, Tayebi M. Production, and characterization of cobalt/vanadium boride nanocomposite powder by mechanochemical method. Materials Chemistry and Physics 202 (2017) 251–257.
20. Wu C, Bai Y, Wang X, Wu F, Zhang C. Comparisons of Co-B alloys synthesized via different methods for secondary alkaline batteries. Solid State Ionics 179 (2008) 924–927.
21. Doñu-Ruiz MA, López-Perrusquia N, Renteria-Salcedo A, Flores-Martinez M, Rodriguez-De Anda E, Muhl S, et al. Tribocorrosion behavior of boride coating on CoCrMo alloy produced by thermochemical process in 0.35% NaCl solution. Surface and Coatings Technology 425 (2021) 127698.
22. Simsek T, Barış M, Akkurt A. Co2B nanopartikülleri ile kaplanmış S235JRC karbon çelik malzemelerin farklı kesme yöntemleri ile işlenebilirlik özelliklerinin araştırılması. Journal of Polytechnic 22(1) (2019) 169–177.
23. Khoshsima S, Altıntaş Z, Burkhardt U, Schmidt M, Prashanth KG, Somer M, et al. CoB-TiB2 crystalline powders: Synthesis, microstructural analysis and their utilization as reinforcement agent. Advanced Powder Technology 31 (2020) 2964–2972.
24. Altıntaş Z, Khoshima S, Somer M, Balcı Ö. The synthesis of binary and ternary cobalt-based metal borides by inorganic molten salt technique. Journal Boron 5(1) (2020) 12–22.
25. Yolcular S, Karaoglu S. Hydrogen generation from sodium borohydride with cobalt boride catalysts. ALKU Fen Bilim Dergisi 2(2) (2020) 84–96.
26. Yılmaz D, Savacı U, Koç N, Turan S. Investigation of Boro/carbothermic and carbothermic reduction synthesized calcium hexaborides. Journal of Boron 3(2) (2018) 103–108.
27. Balcı, Özge AD. Borür-Karbür esaslı kompozit tozların öşütme destekli karbotermik redüksiyon yöntemi ile ekonomik yoldan üretimi. Metalurji 178 (2016) 40–44.
28. Verma PC, Mishra SK. Synthesis of iron boride powder by carbothermic reduction method. Materials Today: Proceedings 28 (2019) 902–906.
29. Yucel O, Addemir O, Tekin A. The optimization of parameters for the carbothermic production of ferroboron. Paper presented at proceedings of the 6th international ferroalloys congress, Cape Town, pp. 285–289, 1992.

30. Ross JRH. Catalyst Characterization in: Ross JRH (Eds) Contemporary Catalysis fundamentals and current applications, Elsevier, Amsterdam, pp.121–132, 2019.
31. Faria MIST, Leonardi T, Coelho GC, Nunes CA, Avillez RR. Microstructural characterization of as-cast Co-B alloys. Materials Characterization 58 (2007) 358–62.
32. Petit C, Pileni MP. Nanosize cobalt boride particles: Control of the size and properties. Journal of Magnetism and Magnetic Materials 166 (1997) 82–90.
33. Baris M, Simsek T, Akkurt A. Mechanochemical synthesis and characterization of pure Co2B nanocrystals. Bulletin of Materials Science 39(4) (2016) 1119–1126.